공학석사학위논문

연소기와 터빈 상호작용이 가스터빈 노즐베인 공력 성능에 미치는 영향에 대한 실험적 연구

Experimental investigation of the effects of combustor turbine interaction on the aerodynamic performance of a gas turbine nozzle vane

2021년 2월

서울대학교 대학원

기계공학부

지 창 은

연소기와 터빈 상호작용이 가스터빈 노즐베인 공력 성능에 미치는 영향에 대한 실험적 연구

Experimental investigation of the effects of combustor turbine interaction on the aerodynamic performance of a gas turbine nozzle vane

지도 교수 황 원 태

이 논문을 공학석사 학위논문으로 제출함
2020년 10월

서울대학교 대학원
기계공학부
지 창 은

지창은의 공학석사 학위논문을 인준함
2020년 12월

위 원 장 최 해 천 (인)

부위원장 황 원 태 (인)

위 원 김 호 영 (인)

Abstract

In order to understand turbine aerodynamic performance, cascade experiments have been utilized by many researchers. However, in most experiments, only the turbine section is investigated, and the complex flow field exiting the combustor is not taken into account. Thus, the aerodynamic characteristics will not fully reflect those of the actual turbine.

In this research, a combustor simulator consisting of 1 swirler and ten dilution holes is employed before the turbine cascade. A custom-designed wind tunnel is used to supply the main flow through the swirler, and secondary flow through the dilution holes on the outer and inner combustor liner. The experiment was conducted by controlling the flow rates of the main flow and secondary flow using a section divider in the diffuser of the wind tunnel. The velocity and total pressure field at the entrance and exit of the cascade are measured by a 5 hole probe.

Flow rotating counterclockwise was observed at the cascade entrance, and a passage vortex structure was detected at the exit. Due to the swirl effect and asymmetry of the liner angle, the loss coefficient distribution differs between the upper and lower section based on mid span. As the average mass flow rate through the dilution holes increases, the loss coefficient and swirl number increase, but profile loss decreases.

Keyword : Gas turbine, Aerodynamic loss, Turbine cascade, Combustor simulator, Dilution hole flow, Loss coefficient, Profile loss
Student Number : 2019-29557

Table of Contents

List of Figures

List of Tables

Nomenclature

A	Area of dilution hole
C	Chord length of vane
C_x	Axial chord length of vane
D_1	Dilution holes close to wind tunnel
D_2	Dilution holes close to cascade
H	Span height
L	Chord length of vane
$\dot{m}$	Bulk mass flow rate at dilution hole
N	Error test quantity
$\hat{n}$	Unit vector normal to the surface
P_t	Total pressure
Re	Reynolds number based on chord length of vane
R	Radial coordinate
$\bar{r}$	Hydraulic diameter
SW	Swirl number
S	Pitch length
U	Streamwise direction velocity
u	Average fluid velocity
V	Spanwise direction velocity
$V_{mixedout}$	Averaged velocity of outlet
$\lvert\vec{V}\rvert$	Magnitude of velocity
v	Velocity at center of dilution hole
v_θ	Tangential velocity
$\vec{v}$	Velocity vector

Y_p	Loss coefficient
W	Pitchwise direction velocity
x	Streamwise direction
y	Spanwise direction
z	Pitchwise direction
α	Pitch angle
β	Yaw angle
ρ	Fluid density
λ	Stagger angle
θ_{up}	Angle of the upper plate of the section divider
θ_{down}	Angle of the lower plate of the section divider
μ	Air dynamic viscosity
$()_{inlet}$	Value of inlet of the cascade
$()_{outlet}$	Value of outlet of the cascade
$()^m$	Mass averaged value

Chapter 1. Introduction

1.1. Research background

Gas turbine performance is highly dependent on the aerodynamic characteristics of the turbine section. Therefore, research on aerodynamic performance to increase gas turbine efficiency is essential when developing gas turbines.

Many researchers have utilized cascade experiments for aerodynamic analysis of turbine blades. Ainley and Mathieson [1] summarized various experimental studies on pressure loss, which investigated variables such as the blade profile, Reynolds number, Mach number, and incidence angle. Through their analysis, an equation that later became a well known criterion for turbine loss correlation was derived. Harrison [2] estimated the profile loss and secondary loss in a linear cascade via total pressure and velocity measurements. Heyes et al. [3] found that the pressure loss increased as the blade tip clearance ratio and chord length increased. However, turbine inlet characteristics are significantly different from uniform inlet flow, making it difficult to predict an actual turbine's aerodynamic performance.

To take into consideration the characteristics of the actual flow entering the turbine, recently various studies have examined methods to simulate the exit flow of the combustor. The effects of turbulence intensity, swirl, and dilution hole flow on the downstream

turbine cascade have been actively examined. Simoni et al. [4] conducted a study on the effect of unsteady inflow generated under realistic turbine conditions on profile loss by generating a wake at the turbine inlet. The effect of wake parameters on the turbulence intensity and wake momentum deficit related to the loss was found. Studies related to swirl flow have also been conducted. Shih and Lin [5] investigated aerodynamic loss and swirl strength for different turbine vane leading edge shapes. This study revealed that the turbine inlet swirl structure could reduce stagnation pressure losses and heat transfer to the airfoil surface for similar leading edge shapes. A change in the pressure loss coefficient according to the presence of the swirler, and how it affected aerodynamic loading, has also been observed [6]. Another study confirmed the change in aerodynamic loss and flow angle according to the swirl number [7].

Some researchers have studied the effect of dilution hole flow on aerodynamic loss. It was found that the flow field, turbulence strength, and aerodynamic characteristics showed a massive difference depending on the flow rate through the dilution holes [8]. Additionally, through CFD, it was shown that the loss varies depending on the flow rate in the combustor simulator with liner dilution holes and film cooling holes [9].

There have also been some domestic studies on the aerodynamic loss within a turbine cascade. Song et al. [10] analyzed the loss mechanism and rheological structure for a two-stage axial

turbine. Analyses of the vortex flow structure and relative total pressure were used to investigate the mechanism by which abnormal losses occur. Lee et al. [11] confirmed the 3D flow and pressure loss downstream of the turbine stator under uniform inlet flow conditions. However, few studies have been conducted by simulating both the swirler and the dilution holes in a combustor simulator based on an actual combustor.

1.2. Purpose of research

In this study, we experimentally study how the outlet flow field of the combustor affects the aerodynamic performance of the turbine nozzle vane. To simulate realistic turbine inlet flow conditions, a combustor simulator is installed in front of a turbine vane cascade. A custom-designed wind tunnel has been built, which supplies the main flow through the swirler, and also secondary flow through the liner dilution holes. To analyze the vane aerodynamic performance, the velocity field and total pressure field in the entrance and exit planes of the cascade are measured with a 5 hole probe. Based on this, a comparative analysis of the loss coefficient, profile loss, and swirl number related to aerodynamic performance is conducted.

Chapter 2. Experimental method

2.1. Wind tunnel

Figure 2.1 is a schematic of the wind tunnel, consisting of a blower, diffuser, heater, mesh & settling chamber, contraction, and test section. An 18.5 kW blower supplies air at ambient conditions at a fixed volume flow rate of 165 m^3/min at maximum revolutions per minute (RPM). Unlike conventional wind tunnels, the flow rates to section 1, 2, and 3 can be adjusted through a section divider within the diffuser. The flow in section 2 corresponds to the main flow through the combustor swirler, and the flow entering sections 1 and 3 provide secondary flow through the dilution holes. The heater has a maximum capacity of 50 kW, and can raise the air temperature to 80 degrees Celsius. The width of the contraction is 400 mm, and the height of section 1, 2, 3 is 240 mm, 260 mm, and 240 mm, respectively. The settling chamber contains three mesh and one honeycomb, which stabilizes the flow and makes it uniform. The actual picture of the wind tunnel is in Figure 2.2.

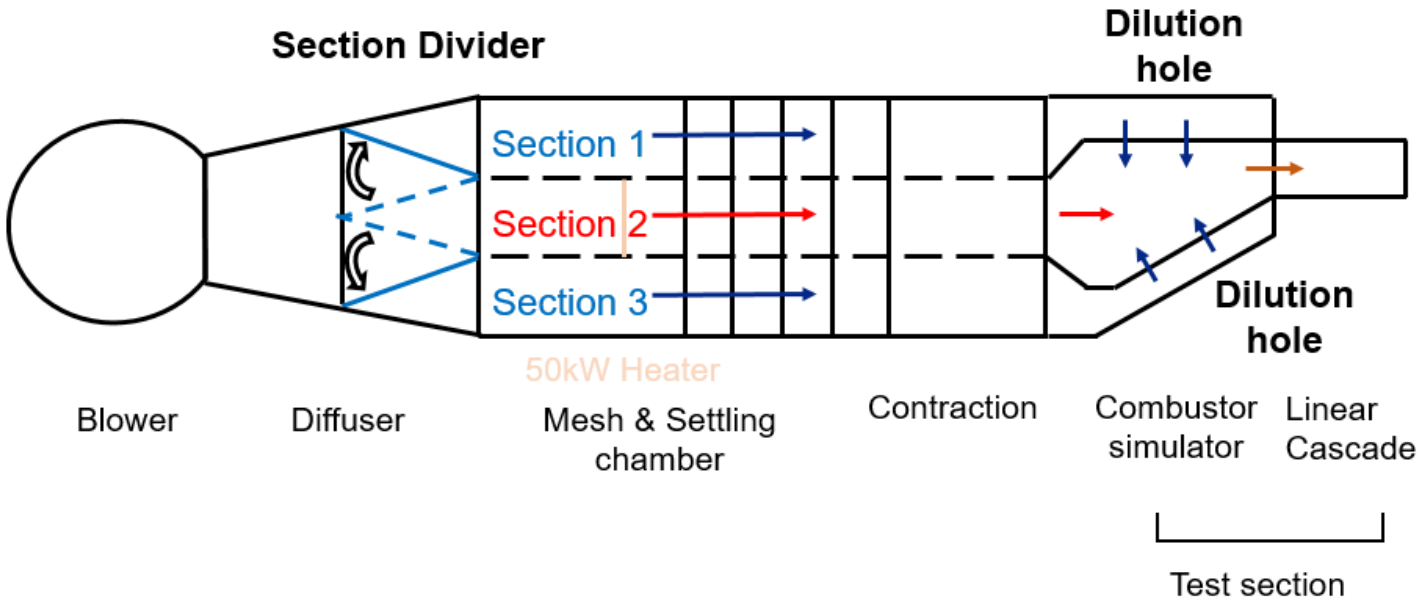

Figure 2.1 Schematic of wind tunnel

Figure 2.2 Custom-designed wind tunnel

2.2. Test section

The test section is divided into two parts: combustor simulator and turbine nozzle cascade. A schematic is shown in Figure 2.3, and a photograph of the test section is shown in Figure 2.4. The combustor simulator represents an actual combustor model, and consists of a 1 cup swirler and 5 dilution holes on both the inner and outer liners. The flow from the swirler and dilution holes are mixed within the simulator, and then enter the cascade. The swirler is in the shape of a dual annular counter rotating swirler (DACRS), and is made of Duraform Prox PA nylon material by Selective Laser Sintering (SLS) 3D printing. The rest of the combustor simulator is entirely made of aluminum. The outer liner (OL) is horizontal and the inner liner (IL) is at 22.15 degrees relative to the ground. For the dilution holes, the two close to the swirler are termed D_1, and the three close to the cascade are termed D_2. The x−axis is the streamwise direction, the y−axis is the span (i.e. radial) direction, and the z−axis is the pitch (i.e. circumferential) direction.

The turbine cascade is a two−passage cascade comprised of three vanes. The vane shape was obtained by extruding the mid span of a representative nozzle guide vane. It was manufactured with the same method and material as the swirler. An adjustable tailboard is installed behind the vane. The details of the vane configuration are shown in Figure 2.5 and Table 2.1. The span length was scaled up to 200 mm, and the rest of the parameters were adjusted accordingly.

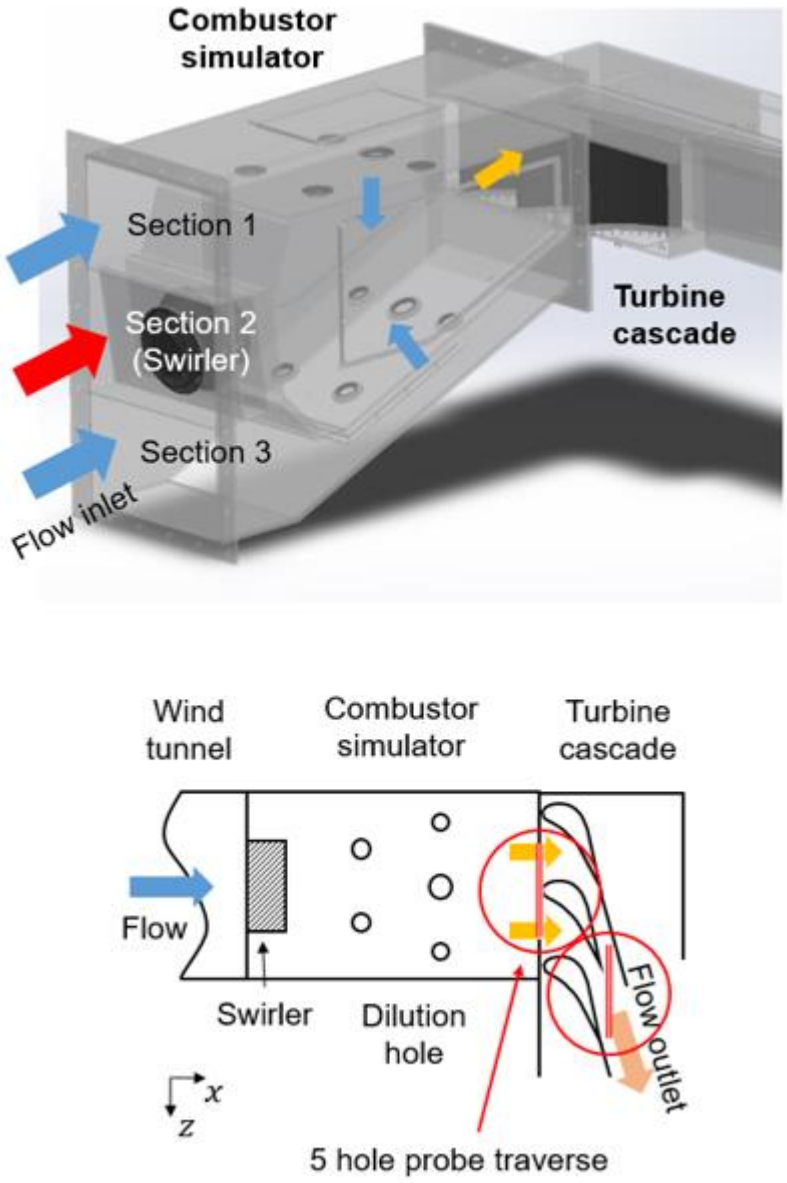

Figure 2.3 CAD model of test section (top) and experimental setup schematic (bottom)

Figure 2.4 Photograph of test section

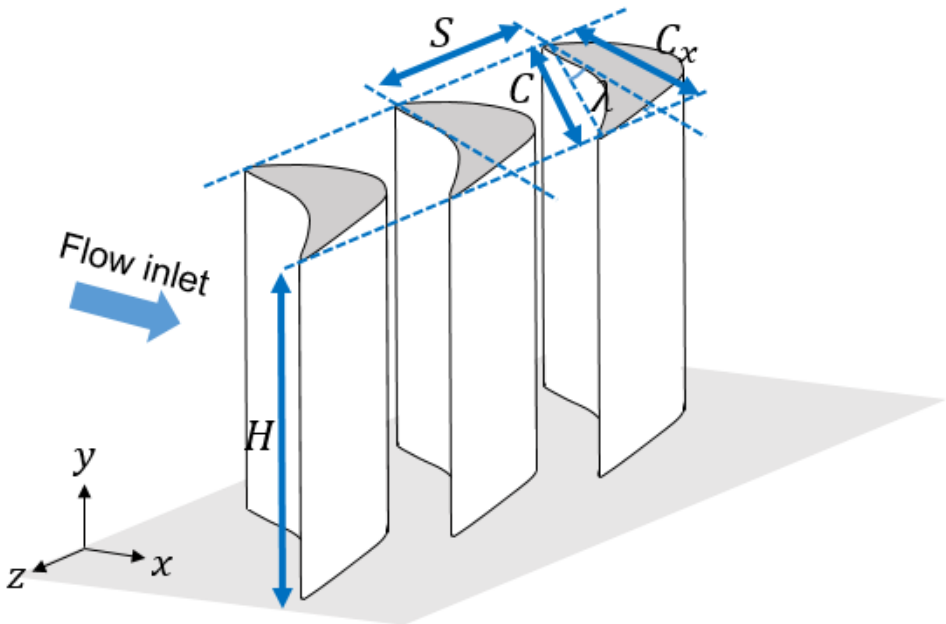

Figure 2.5 Schematic of the vane

Table 2.1 Geometric parameters of the vane

Nozzle guide vane	
Chord length, C	232.16 mm
Axial chord length, C_x	140.86 mm
Stagger angle, λ	52.65°
Span, H	200 mm
Pitch, S	179 mm
Solidity, C/S	1.16

2.3. Test matrix and measuring locations

The experiment was conducted by adjusting the angles between the upper and lower planes of the wind tunnel section divider and the horizontal plane, θ_{up} and θ_{down}. This affects flow split between dilution holes and main flow. Although the main flow is reduced, dilution hole flow is increased, so the overall flow entering the cascade is the same. A total of 4 $\theta_{up}/\theta_{down}$ section divider angle cases were tested: (a) 10° / 10°, (b) 9.5° / 9.5°, (c) 9° / 9°, (d) 8° / 8°. In all cases, the Reynolds number based on the chord length is fixed at 154,000, which is lower than 300,000 of the actual engine condition. Since there is a difference compared to the actual engine case, the type of losses that can be observed is limited. However, the profile loss, which is one of the main targets of this research and occupies 30~70% of the overall loss, is not significantly affected by this change in Reynolds number [15], so conducting the tests at this lower Reynolds number was justified.

Measuring locations are shown in Table 2.3. An L-shaped 5 hole probe from Vectoflow was utilized for the experiment. The details of the 5 hole probe are shown in Table 2.4 and Figure 2.6. The velocity of the flow from the dilution holes, and the main flow velocity and total pressure at the cascade's entrance plane (at 0.1 C_x upstream from the leading edge) and exit plane (at 1.3 C_x downstream from the leading edge) were measured. The measurement area for the entrance and exit planes is 200 mm in width and 190 mm in height,

centered at the vane. The probe is connected to a Scanivalve DSA3217 pressure scanner.

Table 2.2 Measurement locations

Measurement location		Instrument
Dilution holes	Outer liner velocity magnitude	5 hole probe
	Inner liner velocity magnitude	
Cascade	Upstream 2D3C velocity	
	Upstream total pressure	
	Downstream 2D3C velocity	
	Downstream total pressure	

Table 2.3 Geometric information of 5 hole probe

Model	5 hole probe
Type	L-shaped
Length	250 mm
Head shape	Conical
Head diameter	3 mm
Material	Stainless steel

Figure 2.6 Photograph of 5 hole probe

2.4. Data reduction

The Reynolds number is defined as

$$\mathrm{Re} = \frac{\rho u L}{\mu} \quad (1)$$

where ρ is the air density, U is the average air velocity at the vane leading edge, L is the chord length of the vane, and μ is the dynamic viscosity of air.

The mass flow rate at the dilution hole is defined as

$$\dot{m} = \rho A v \quad (2)$$

where A is the area of the dilution hole, and v is the velocity at the center of the dilution hole.

The loss coefficient Y_p is calculated in terms of the difference between total pressure at the inlet and outlet of the cascade, and the averaged velocity of outlet V_{mixed}.

$$Y_p = \frac{P_{t,inlet} - P_{t,outlet}}{\frac{1}{2}\rho {V_{mixed}}^2} \quad (3)$$

The mass averaged loss coefficient is defined as

$$\overline{Y_p}^m = \frac{P_{t,inlet} - \overline{P_t}^m}{\frac{1}{2}\rho V_{mixed}{}^2} \quad \text{, where } \overline{P_t}^m = \frac{\int \rho u P_t dA}{\int \rho u dA} \qquad (4)$$

The profile loss is the loss caused by the boundary layer of the vane. It was calculated by Ainley and Mathieson [1] by setting the minimum value among the pitch-wise averaged loss coefficients of the trailing edge of the vane.

The swirl number is defined as

$$S = \frac{\int_S r v_\theta (\vec{v} \cdot \hat{n}) dS}{\bar{r} \int_S v_x (\vec{v} \cdot \hat{n}) dS} \qquad (5)$$

where r is the radial coordinate, v_θ is the tangential velocity, $\vec{v}$ is the velocity vector, $\hat{n}$ is a unit vector normal to the inlet surface of the cascade, S is the inlet area of the cascade, and $\bar{r}$ is the hydraulic diameter. The swirl number is the ratio of the tangential momentum flux to axial momentum flux.

The local velocity and total pressure are obtained at intervals of 10 mm in the y and z direction, using a dual-axis traverse system. Measurements were made at a total of 420 points per plane. For repeatability, measurements were performed 15 times per point, and average values were used for the velocity and total pressure.

2.5. Uncertainty

Uncertainty analysis is performed using the method described by Moffat [12]. The uncertainty of the 5 hole probe depends on (i) errors in measuring velocity and (ii) errors in measuring the angle. Error evaluation was performed at 0.3 Mach number and 210 times by Vectoflow. Figure 2.7 shows the histograms of the error evaluation of yaw angle (α), pitch angle (β), and velocity magnitude, respectively, from the left. The orange line represents the standard deviation of each variable, and N represents the error. The standard deviation of the velocity magnitude is 0.13 m/s. The standard deviation of the pitch and yaw angle is 0.13° and 0.22°, respectively.

The uncertainty in V_{mixed}, $P_{t,inlet}$, $P_{t,outlet}$ are 0.25%, 2.51%, and 2.48%, respectively. Therefore, the uncertainty in the loss coefficient is calculated by equation (6), and results in 3.52%.

$$\delta Y_p = \left\{ \left(\frac{\delta P_{t,inlet}}{\frac{1}{2}\rho {V_{mixed}}^2} \right)^2 + \left(\frac{\delta P_{t,outlet}}{\frac{1}{2}\rho {V_{mixed}}^2} \right)^2 + \left(\frac{(P_{t,inlet} - P_{t,outlet})}{\frac{1}{4}\rho {V_{mixed}}^3} \delta V \right)^2 \right\}^{1/2} \quad (6)$$

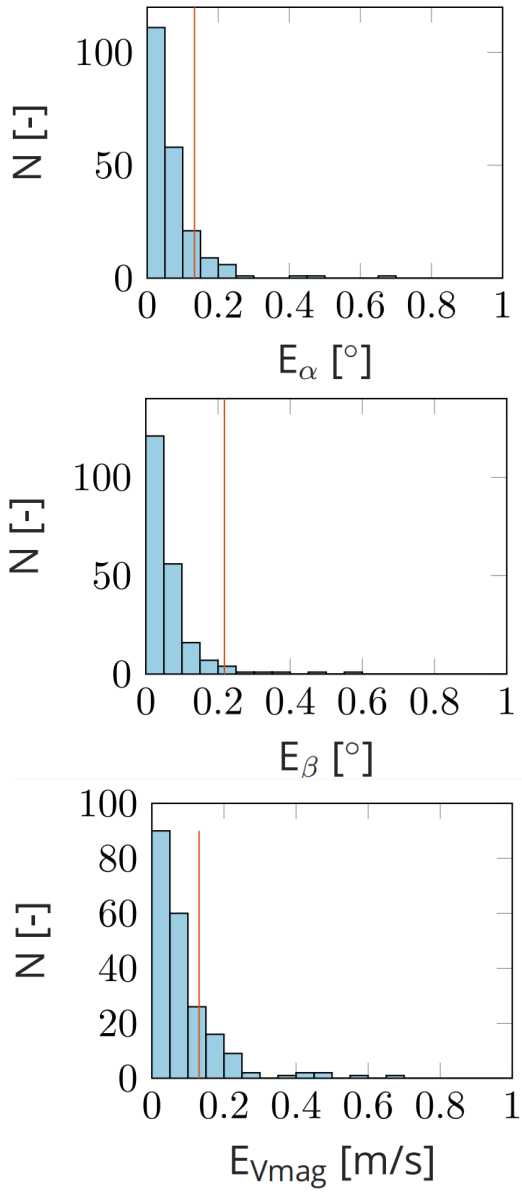

Figure 2.7 Histograms of errors evaluated on test points

Chapter 3. Results and Discussion

3.1. Dilution hole mass flow rate

The mass flow rate was calculated by measuring the velocity at the center of the dilution hole using the 5 hole probe. The 5 hole probe was inserted through a port on the side of the combustor simulator. The dilution hole mass flow rate for the section divider configuration is shown in Table 3.1. The zones are divided into row 1 and 2 of the inner liner and outer liner, respectively, resulting in a total of 4 zones. The mass flow rate of each zone is organized by the section divider angle.

As the section divider's angle is decreased, the flow rate of the secondary flow in section 1 and 3 of the wind tunnel naturally increases, so the mass flow rate from each dilution hole increases. In addition, it was confirmed that the mass flow rate was lower at the inner liner for all angle cases. This implies that the liner angle has an adverse effect in regards to the pressure drop through the dilution hole.

Table 3.1 Dilution hole mass flow rate

Total $\dot{m}$ (g/s)				
Section divider angle $(\theta_{up}/\theta_{down})$	(a) 10°/ 10°	(b) 9.5°/ 9.5°	(c) 9°/ 9°	(d) 8°/ 8°
① D_{1OL}	107.76	114.39	117.05	132.08
② D_{2OL}	169.50	169.09	176.25	201.85
Outer liner (① + ②)	277.26	283.48	293.30	333.93
③ D_{1IL}	73.22	86.97	107.80	122.35
④ D_{2IL}	109.17	115.42	151.58	182.90
Inner liner (③ + ④)	182.39	202.39	259.38	305.25
Averaged outer liner and inner liner	229.83	242.94	276.34	319.59

3.2. Flow structure

The flow structure in the entrance and exit plane of the cascade is shown in Figures 3.1 to 3.5. The dotted line in the middle of the contour indicates the vane leading edge location, and the suction side (SS) and pressure side (PS) are indicated at the left and right, respectively. The top of each contour is the region toward the turbine casing, and the bottom is the hub region. Figures 3.1, 3.2, 3.3, and 3.4 correspond to the dimensionless U, V, W velocity (x, y, z direction), and velocity magnitude contour at the entrance for all cases, respectively. Figure 3.5 shows the dimensionless U velocity contour at the exit plane for all cases, and the secondary flow is displayed in vector form.

For all cases, a similar flow structure exists. Figures 3.1 and 3.4 show that the streamwise velocity is the most dominant component for the velocity magnitude, and the velocity increases from the center to the edge. Through Figures 3.2 and 3.3, it was confirmed that the flow rotates in the counterclockwise direction as it enters the turbine. This is a phenomenon caused by the swirler of the combustor simulator. As shown in Figure 3.5, a passage vortex structure is formed in the exit hub region, and a low velocity zone occurs near the suction side because of the shape of the vane. When the data acquisition resolution was increased by 4 times, it was confirmed that the passage vortex structure in the hub region was clearly visible.

As the dilution hole mass flow rate increases, the velocity magnitude at the center of the plane decreases. This is related to the dilution hole mass flow rate. In case (a), the ratio of the mass flow rate between the outer and inner liner is 1.52. However, in case (d), the ratio is 1.09. Because the mass flow rate increase of the inner liner is large, the entire flow from the liner moves in the tip direction. As a result, the flow from the dilution hole tends to move from the center to the edge. Due to this effect, the swirl structure gradually becomes stronger, as is confirmed through Figure 3.4. Table 3.2 shows the swirl number for each case. As a result, the mass flow rate of the dilution hole has a strong influence on the swirl structure in entrance plane of the cascade.

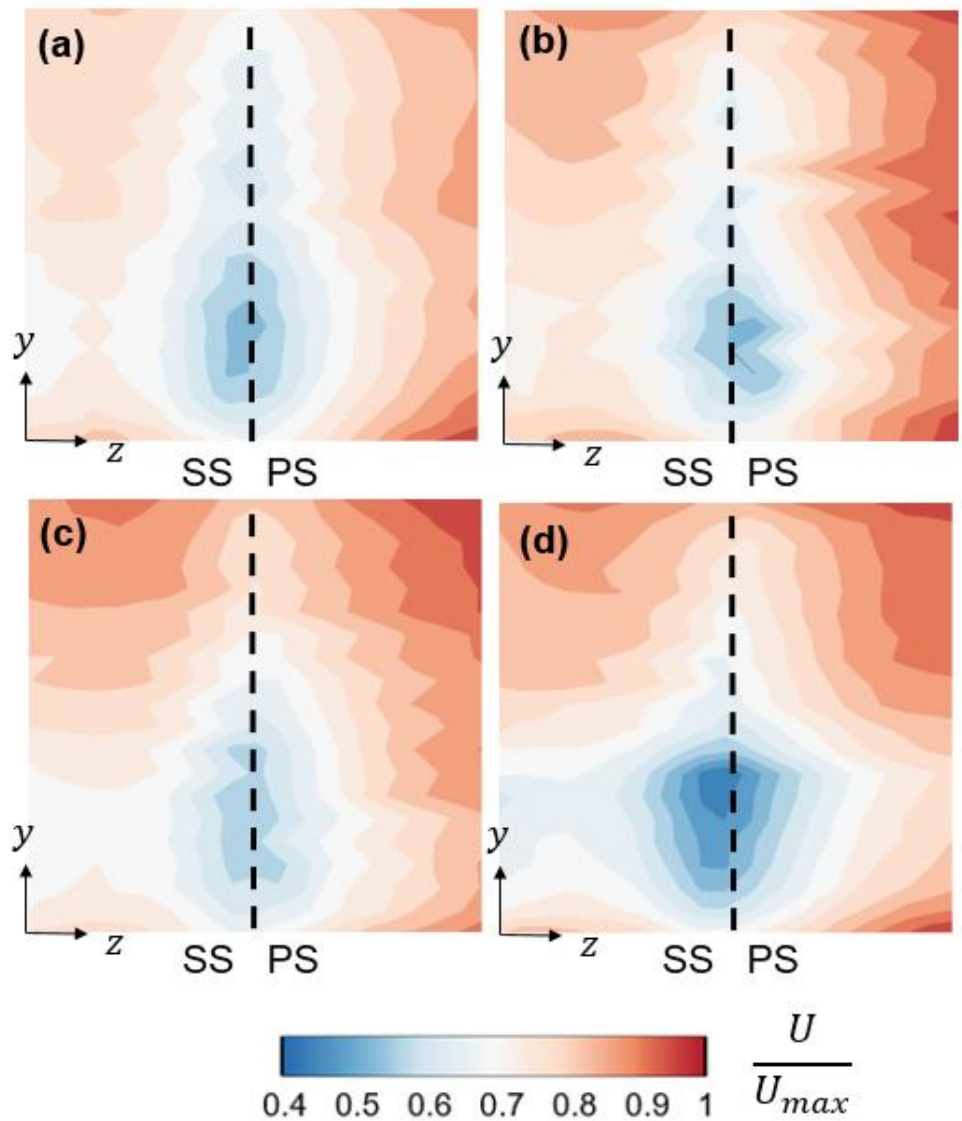

Figure 3.1 Normalized U velocity in the entrance plane

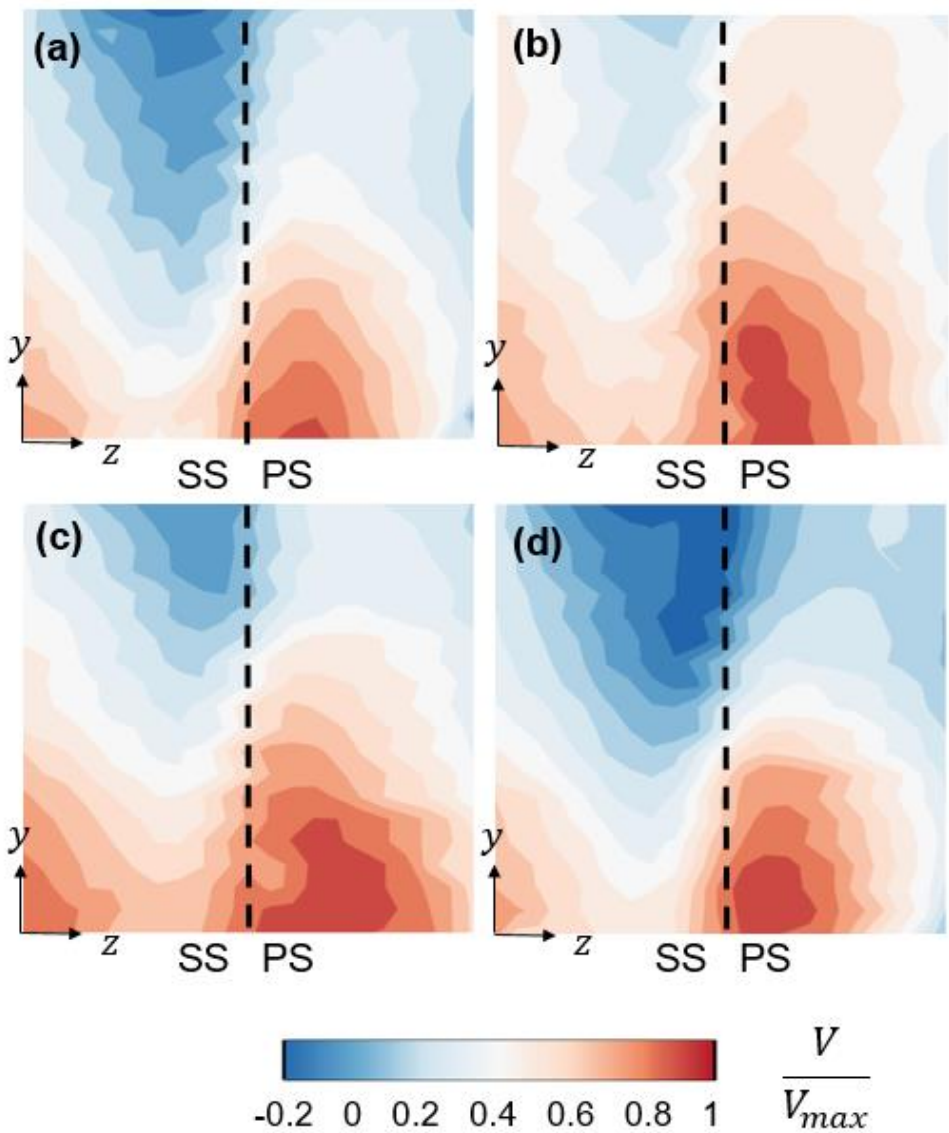

Figure 3.2 Normalized V velocity in the entrance plane

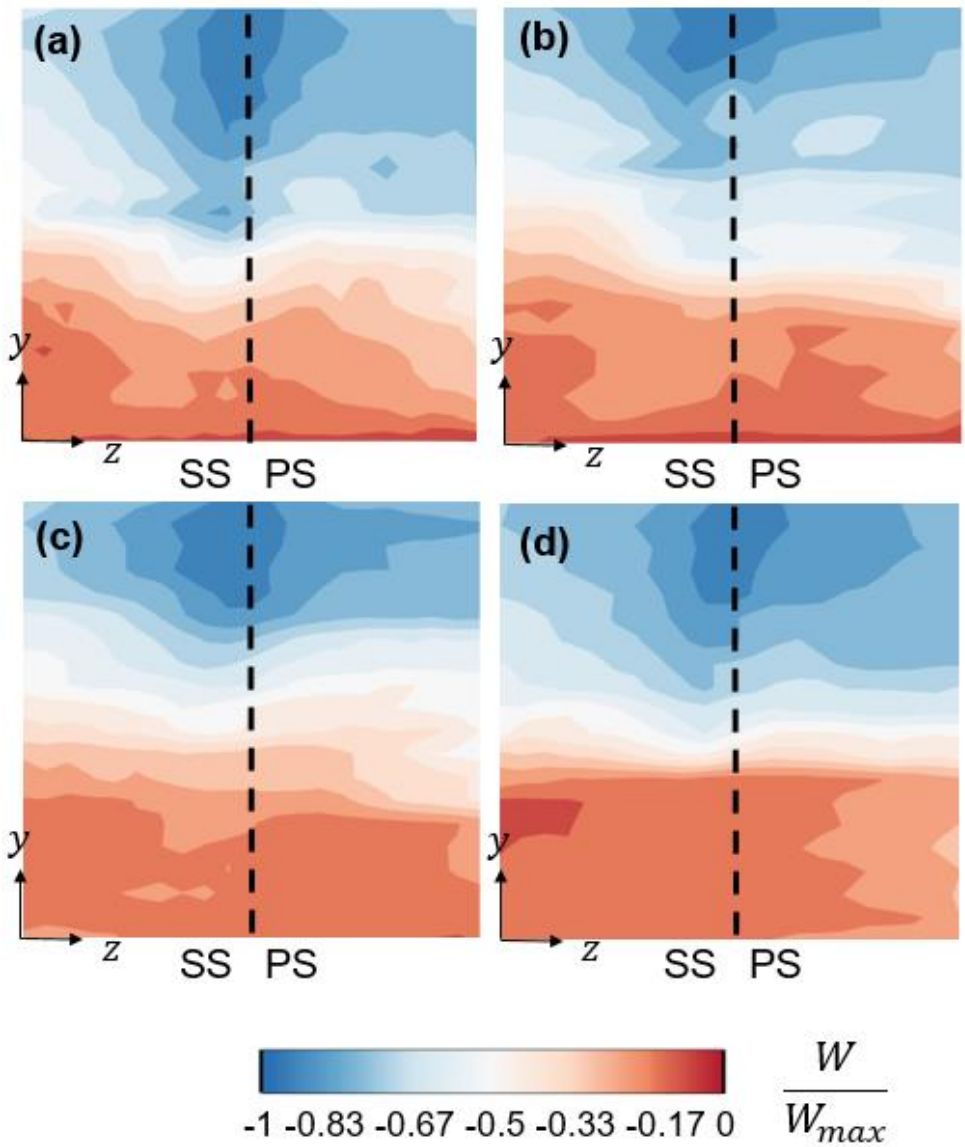

Figure 3.3 Normalized W velocity in the entrance plane

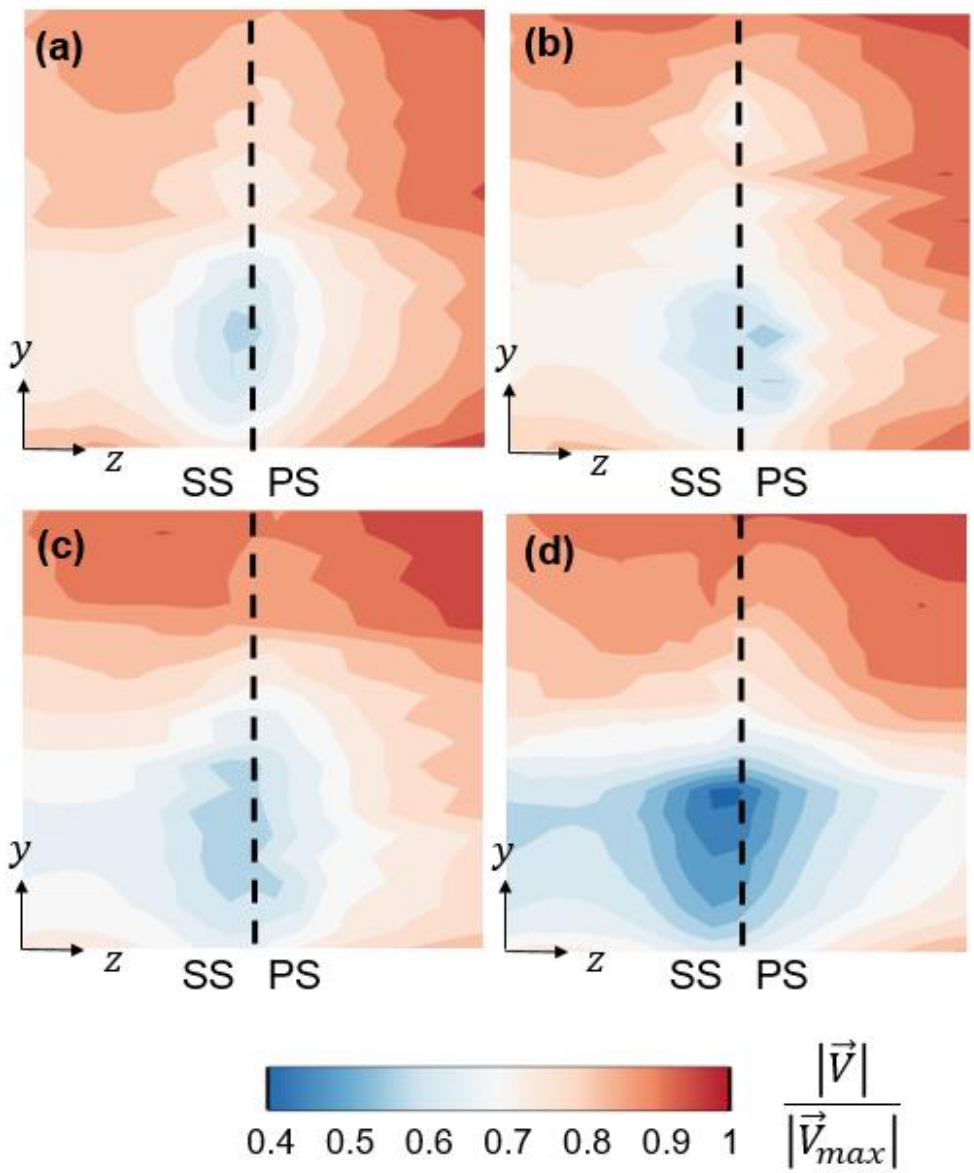

Figure 3.4 Normalized velocity magnitude in the entrance plane

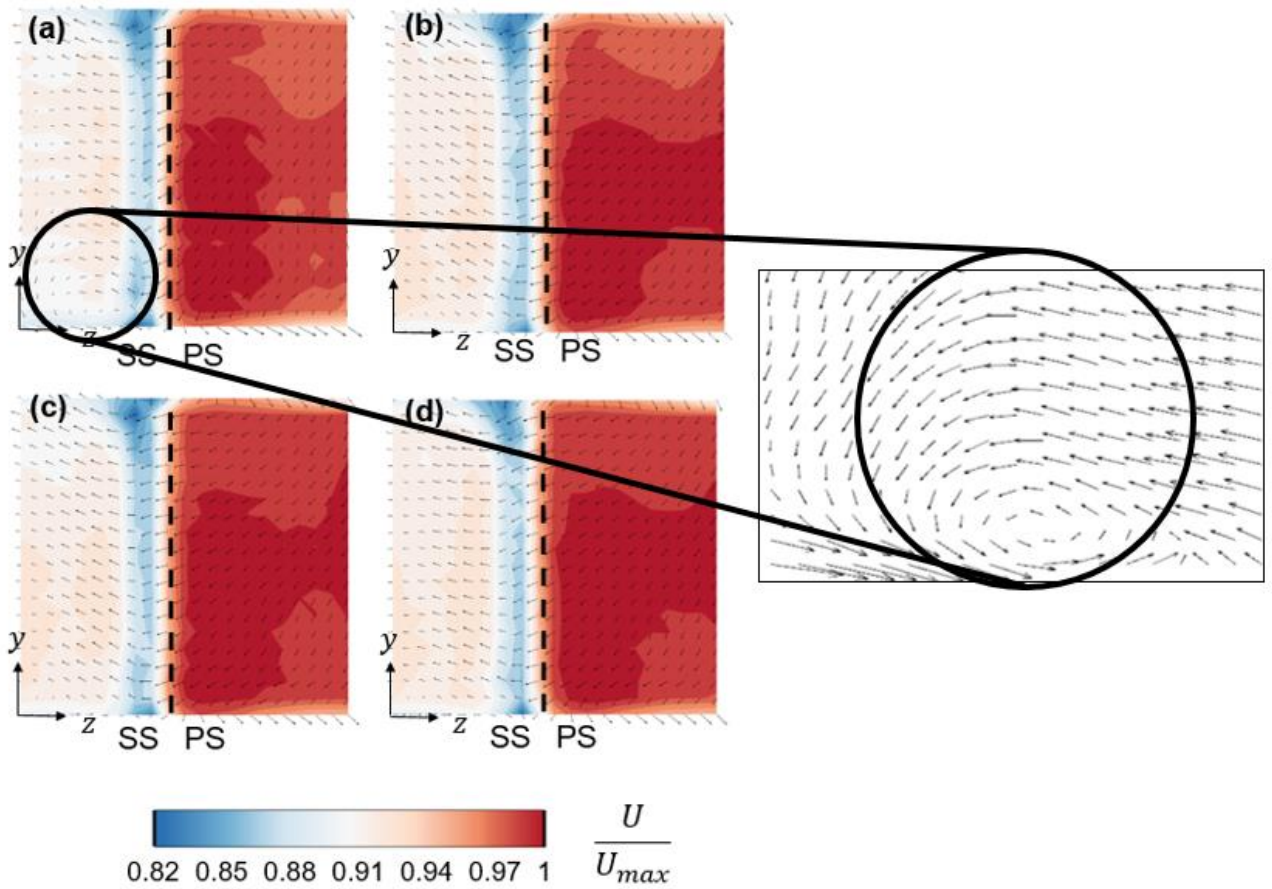

Figure 3.5 Normalized U velocity with secondary flow in the exit plane

Table 3.2 Swirl number in entrance plane

Case	(a)	(b)	(c)	(d)
Averaged mass flow rate through liner (kg/s)	0.230	0.243	0.276	0.320
Swirl number, SW	0.450	0.538	0.556	0.576

3.3. Aerodynamic loss

Figure 3.6 shows the distribution of the loss coefficient for all cases. High loss is observed along the spanwise direction in the suction side due to the vane wake, and low loss is observed in the passage region. The loss core is at the suction side toward the outer casing. The loss coefficient is asymmetrically distributed in the hub and casing regions. Through Figure 3.5, it is observed that the wake toward the casing has a relatively higher velocity deficit, which has a significant effect on the loss.

It can also be seen that larger dilution hole mass flow rate causes a more significant loss core near the casing, with a diminishing loss toward the hub. Barringer et al [13] demonstrated that the loss coefficient increases near the hub due to boundary layer effects, as the ratio of the cooling flow in the combustor outlet flow increases. However, in this study, as the dilution hole mass flow rate increases, the flow rate entering the tip region likely gradually increases due to the swirl. Jacobi et al [14] showed that streamtraces originating from the residual swirl core, and the secondary flow streamtraces originating from the upstream tip endwall boundary layer, meet at the trailing edge. Together, they form the tip loss core. However, this phenomenon does not happen at the hub because of the movement of the stagnation point toward the suction side. This trend well explains that the loss coefficient at the tip region increases, contrary to the hub.

The reason for the large loss towards the tip is conjectured to be due to the two following explanations. First, due to swirl, the inlet flow enters the cascade while rotating counterclockwise. Thus, the incidence angle changes along the vane leading edge in the span direction, and the stagnation position is changed accordingly. Towards the tip, the position of the stagnation point moves to the pressure side, and the flow has to rotate around the leading edge. This causes a thicker boundary layer to develop along the suction side, and can possibly lead to flow separation downstream. On the other hand, towards the hub of the vane leading edge, the boundary layer on the suction side becomes thinner as the stagnation point is pushed to the suction side due to the swirl. Separation is likely suppressed in this region as well.

Second, the jet flow from the dilution holes cause a large local deficit in the streamwise momentum of the main flow as it mixes in the center of the combustor. This local loss region propagates towards the tip region due to the slanted angle of the inner liner, generating a loss core stronger near the tip, compared to the hub.

If the swirl is stronger, the difference in the loss coefficient between the tip and hub region becomes bigger. The area averaged loss coefficient value is shown in Table 3.3. As the secondary flow increases, the swirl number increases, thereby increasing the secondary loss and averaged loss coefficient. Thus, the swirl number and loss coefficient are closely related.

Figure 3.7 shows the pitch-wise distribution of the span-wise mass averaged loss coefficient. In all cases, it was confirmed that the loss was high at the suction side due to the vane shape as mentioned earlier in Figure 3.6. As the dilution hole mass flow rate increases, the increase in the size of the loss core and the decrease in the loss at the hub side cancel each other. Accordingly, the peak values of the mass averaged loss coefficient are similar in all cases.

The left graph of Figure 3.8 shows the loss coefficient in the spanwise direction for the four cases. Profile loss occurs on the blade surface, and is caused by the boundary layer. Previous 2D cascade studies with uniform inlet flow conditions have shown that the loss is the same along the span, which is different from the results of this study. The loss trend of this study displays an asymmetric structure with a large core at the casing region. This is because the flow of the turbine inlet is disturbed by the swirl and dilution hole effects. The loss also increases slightly at the bottom of the hub, due to the hub boundary layer.

The profile loss is shown in Table 3.4. As the dilution hole mass flow rate increases, the profile loss decreases. Since the profile loss corresponds to the minimum pressure loss, this can be confirmed by the left graph of Figure 3.8, where the minimum loss towards the hub region decreases with increasing dilution hole flow. Also, as the dilution hole mass flow rate increases, the loss at the bottom of the hub region decreases. The curves in the left graph of Figure 3.8 can

be shifted so that the minimum loss point is set to 0 in the right graph. This graph shows that the loss is near 0 towards the hub, with some secondary loss occurring at the hub. As the dilution hole mass flow rate increases, it can be clearly seen that the casing region loss increases, relative to the hub region. Since stronger loss occurs near the tip, additional efforts such as adjusting the flow angle are required to reduce this effect.

Figure 3.9 shows the correlation of variables related to the aerodynamic loss for the dilution hole mass flow rate. It was confirmed that the larger the dilution hole mass flow rate, the stronger the swirl structure. Accordingly, the swirl number and averaged loss coefficient increase. However, the profile loss decreases for the same reason.

Table 3.3 Averaged loss coefficient

Case	(a)	(b)	(c)	(d)
Averaged loss coefficient	0.0602	0.0613	0.0676	0.0685

Table 3.4 Profile loss

Case	(a)	(b)	(c)	(d)
Profile loss	0.1828	0.1804	0.1598	0.1233

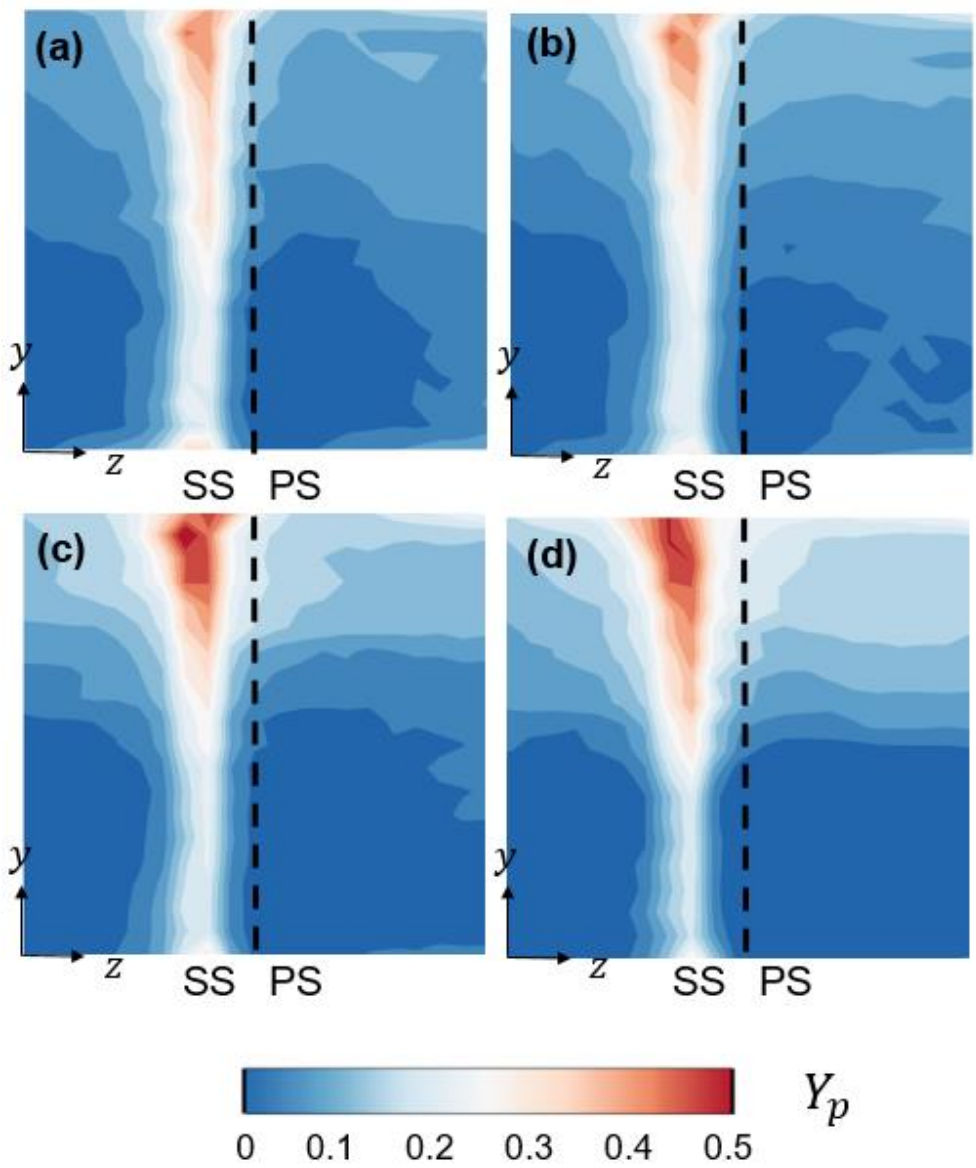

Figure 3.6 Loss coefficient contour

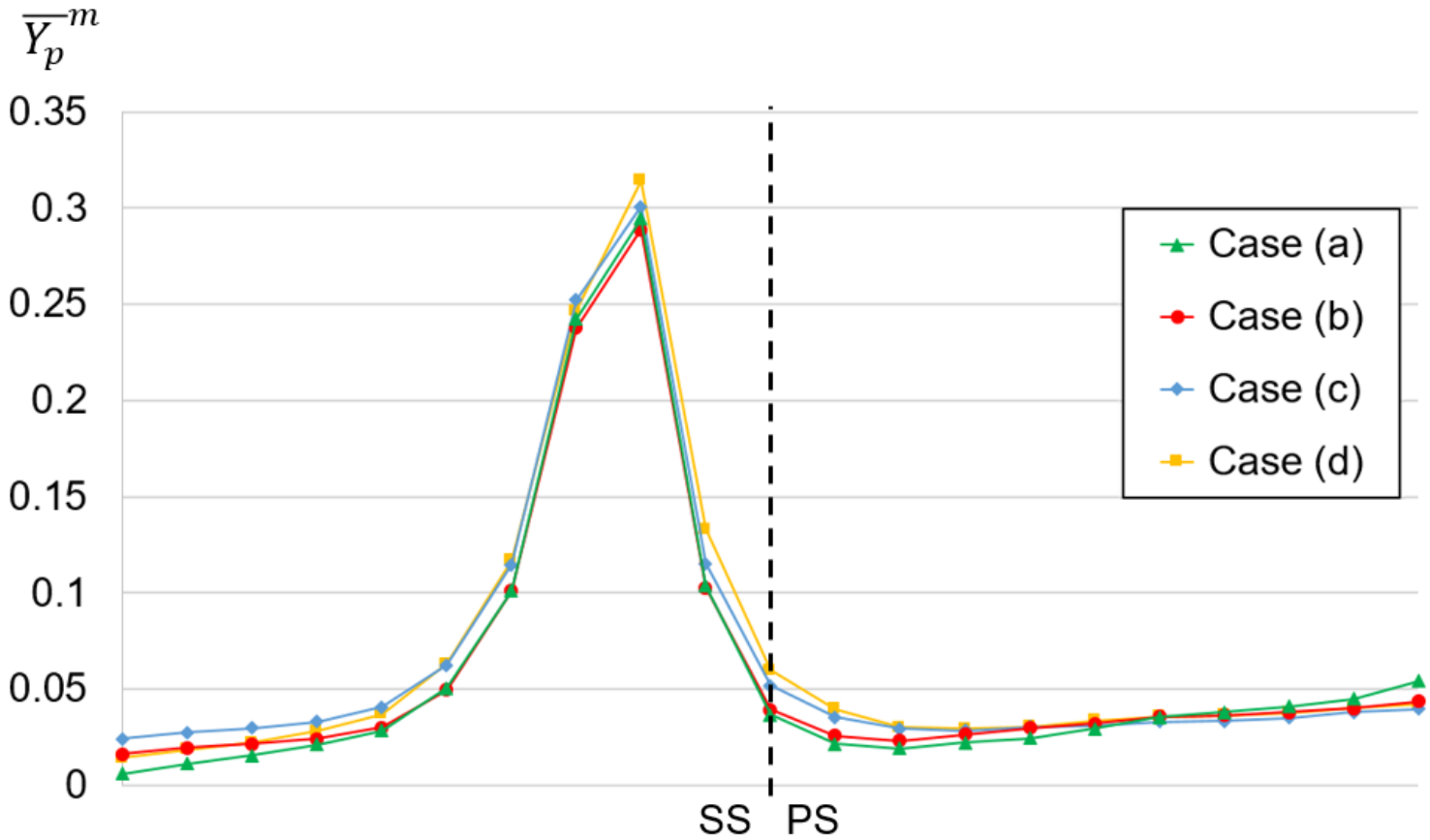

Figure 3.7 Pitch-wise distribution of span-wise mass averaged coefficient

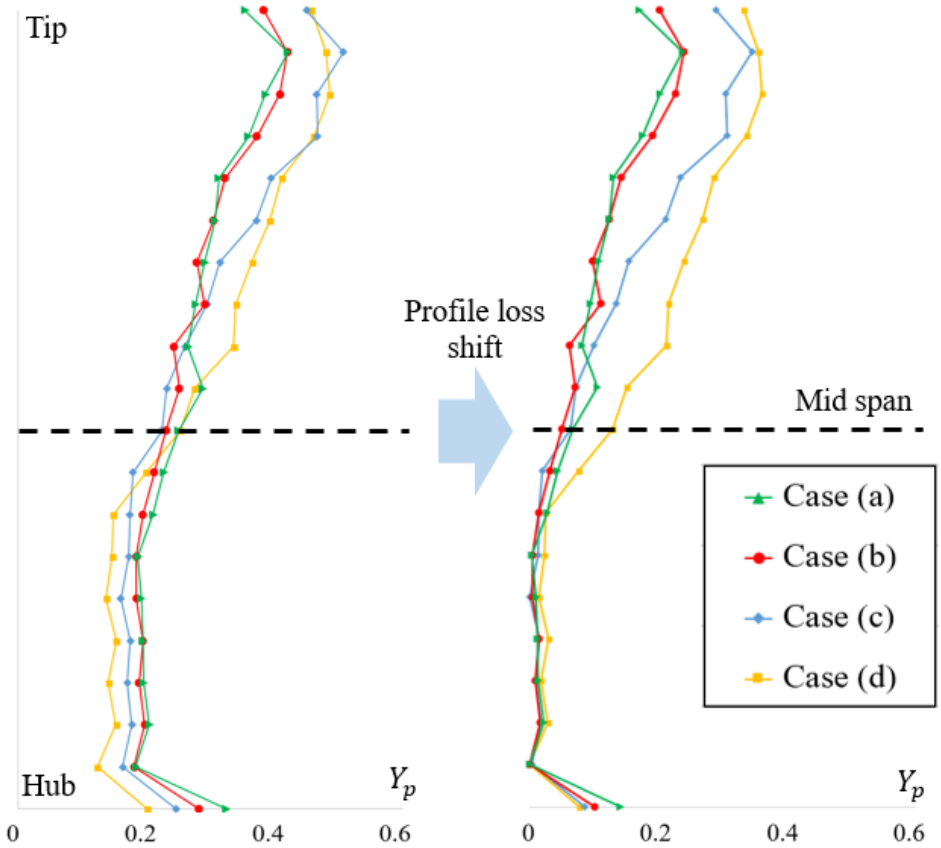

Figure 3.8 Pitch-wise averaged loss coefficient at the trailing edge of the vane

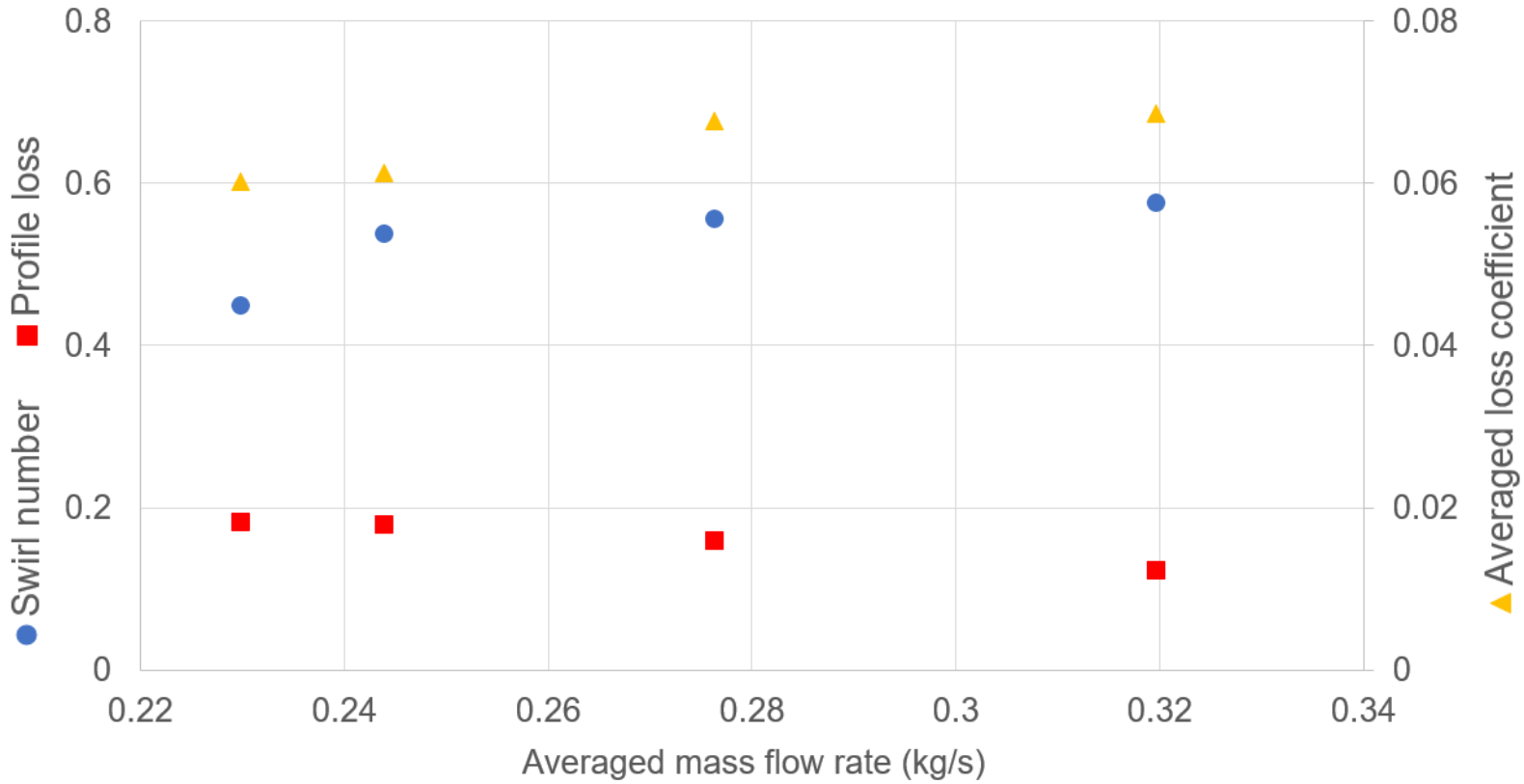

Figure 3.9 Aerodynamic loss correlation

Chapter 4. Conclusion

An experimental study was conducted to confirm the aerodynamic performance and flow field characteristics of a turbine nozzle vane. A custom-designed wind tunnel was constructed, with a single-cup combustor simulator and linear turbine cascade. The mass flow rate from the liner dilution holes was adjusted using the section divider within the diffuser of the wind tunnel. For a total of four cases, the velocity and total pressure at the entrance and exit plane of the cascade were measured by using a 5 hole probe.

As the section divider's angle is decreased, the mass flow rate from each dilution hole increases. The flow rotates in the counterclockwise direction due to swirl at the vane entrance plane, and a passage vortex structure is observed at the suction side hub region in the exit plane. Due to swirl and the slanted inner liner angle, the loss distribution is asymmetric between the hub and casing regions. As the dilution hole mass flow rate increases, the averaged loss coefficient increases, but the profile loss decreases.

Acknowledgement

This work has been supported by the UAV High Efficiency Turbine Research Center program of Defense Acquisition Program Administration and Agency for Defense Development.

Bibliography

[1] Ainley, D. G., and Mathieson, G. C. R., 1955, "An Examination of the Flow and Pressure Losses in Blade Rows of Axial-Flow Turbines," Aeronautical Research Council R. and M. 2891.

[2] Harrison, S., 1990, "Secondary Loss Generation in a Linear Cascade of High Turning Turbine Blades," Journal of Turbomachinery, 112(4), pp. 618-624.

[3] Heyes, F. J. G., Hodoson, H. P., and Dailey, G. M., 1992, "The Effect of Blade Tip Geometry on the Tip Leakage Flow in Axial Turbine Cascades," Journal of Turbomachinery, 114(3), pp. 643-651.

[4] Simoni, D., Yepmo, V., Zunino, P., Ubaldi, M., Lengani, D., and Bertini. F., 2019, "Turbine Cascade Profile Loss Sensitivity to Incoming Wake Parameters: Effects of Reduced Frequency, Wake Momentum Defect and Axial Gap," Proc. ASME Turbo Expo 2019: Turbomachinery Technical Conference and Exposition, American Society of Mechanical Engineers, p. V02AT45A018.

[5] Shih, T. I-P., and Lin, Y.-L, 2002, "Controlling Secondary Flow Structure by Leading Edge Airfoil Fillet and Inlet Swirl to Reduce Aerodynamic Loss and Surface Heat Transfer," Journal of Turbomachinery, 125(1), pp. 48-56.

[6] Qureshi, I., Smith, A. D., and Povey, T., 2011, "HP Vane Aerodynamics and Heat Transfer in the Presence of Aggressive Inlet Swirl," Proc. ASME Turbo Expo 2011: Turbine Technical Conference

and Exposition, American Society of Mechanical Engineers, pp. 1925-1942.

[7] Giller, L. and Schiffer, H. P., 2012, "Interactions Between the Combustor Swirl and the High Pressure Stator of a Turbine," Proc. ASME Turbo Expo 2012: Turbine Technical Conference and Exposition, American Society of Mechanical Engineers, pp. 1401-1415.

[8] Barringer, M. D., Richard, O. T., Walter, J. P., Stitzel, S. M., and Thole, K. A., 2002, "Flow Field Simulations of a Gas Turbine Combustor," Journal of Turbomachinery, 124(3), pp. 508-516.

[9] Kunze, V. R., Wolff, M., Barringer, M. D., Thole, K. A., and Polanka, M. D., 2005, "Numerical Modeling of Flow and Thermal Patterns Within a Combustor Simulator," Proc. ASME Turbo Expo 2005: Power for Land, Sea, and Air, American Society of Mechanical Engineers, pp. 519-528.

[10] Porreca, L., Kalfas, A. I., Abhari, R. S., Yun, Y. I., and Song, S. J., 2009, "Interstage Flow Interactions and Loss Generation in a Two-Stage Shrouded Axial Turbine," Journal of Turbomachinery, 131(1), p. 011002.

[11] Jeong, J. S., Bong, S. W., and Lee, S. W., 2017, "Three-dimensional Flow and Aerodynamic Loss Downstream of First-Stage Turbine Vane Cascade," Trans. of the KSME (B), 41(8), pp. 521-529.

[12] Moffat, R. J., 1988, "Describing the Uncertainties in

Experimental Results," Experimental Thermal and Fluid Science, 1(1), pp. 3-17.

[13] Barringer, M. D., Thole, K. A., and Polanka, M. D., 2004, "Developing a Combustor Simulator for Investigating High Pressure Turbine Aerodynamics and Heat Transfer," Proc. ASME Turbo Expo 2004: Power for Land, Sea, and Air, American Society of Mechanical Engineers, pp. 565-575.

[14] Jacobi, S., Mazzoni, C., Rosic, B., and Chana, K., 2017, "Investigation of Unsteady Flow Phenomena in First Vane Caused by Combustor Flow With Swirl," Journal of Turbomachinery, 139(4), p. 041006.

[15] Coton, T., Arts, T., and Lefebvre, M., 2001, "Effects of Reynolds and Mach numbers on the profile losses of a conventional low pressure turbine rotor cascade with an increasing pitch-chord ratio," Proc. the Institution of Mechanical Engineers Part A, pp. 763-772.

Appendix

This appendix contains the drawing of the experimental setup. Dimensions are in mm unless noted otherwise.

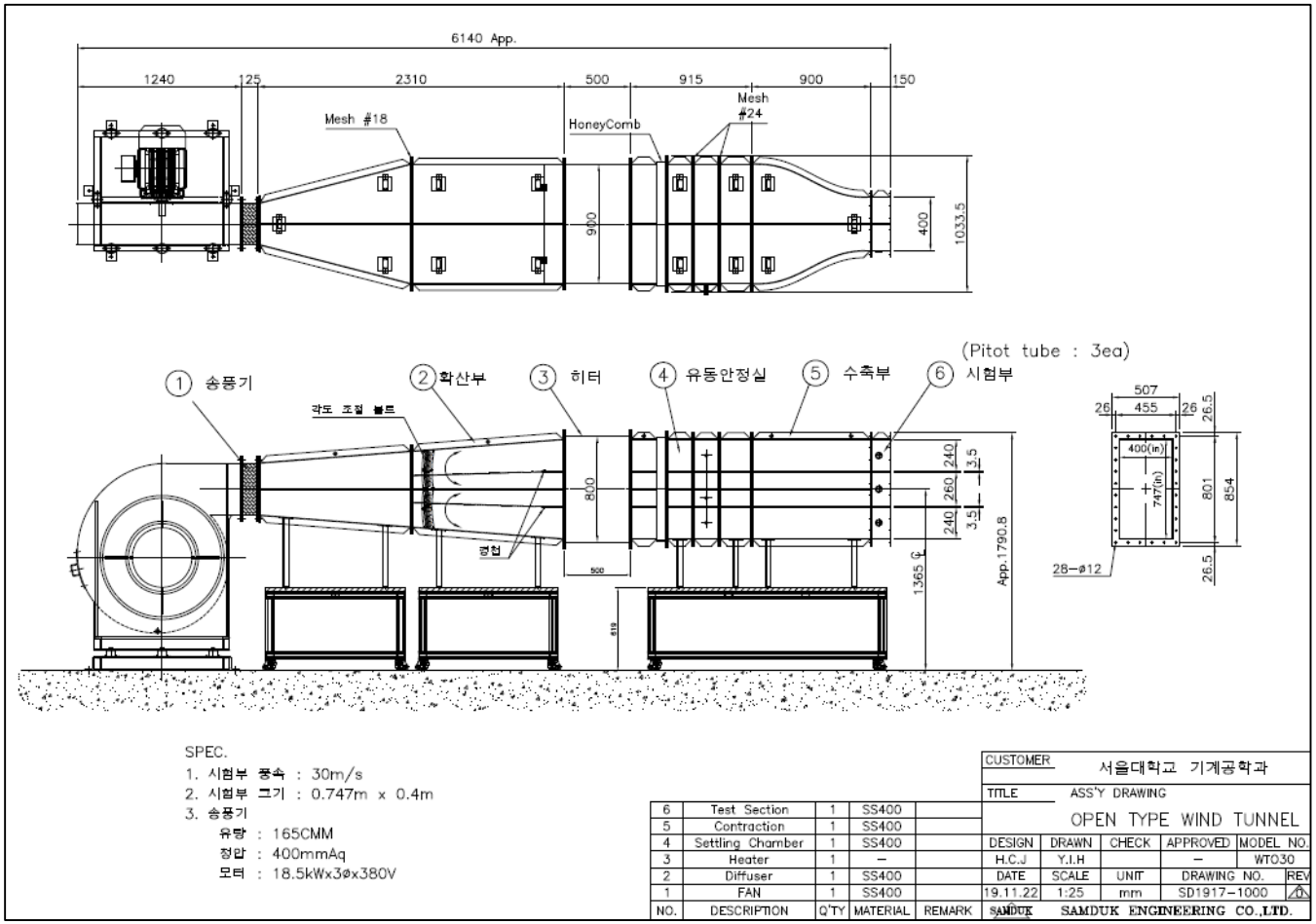

Figure A1. Drawing of open type wind tunnel

요약

가스터빈의 공력 성능을 파악하기 위하여, 캐스케이드 실험은 많은 연구진들에 의하여 연구되었다. 하지만 대부분의 실험에서 터빈부만 관측되었고, 연소기를 빠져나가는 복잡한 유동 장은 고려되지 않았다. 따라서 공력 특성은 실제 터빈의 특성을 완벽하게 반영하지 못한다. 본 실험에서 연소기 모사 장치는 터빈 캐스케이드 전방에 사용된다. 맞춤형으로 설계된 풍동은 스월러를 통한 주 유동과 외부 및 내부 연소기 라이너의 희석공기공을 통하여 2차 유동을 공급하는 데 사용된다. 터빈 캐스케이드 입구와 출구, 연소기 모사 장치의 희석 공기공 중심에서의 속도와 전 압력장을 5공 프로브를 통하여 측정하였다.

입구에서는 반 시계 방향으로 회전하는 유동 구조를 확인하였고, 출구에서는 통로 와류 구조를 관찰하였다. 스월 효과와 라이너 각도 비대칭으로 인하여 손실 계수 분포는 중간 단면을 기준으로 상부와 하부가 다르게 나타났다. 희석공기공의 평균 유질량이 증가함에 따라 큰 스월 구조와 손실 중심의 증가로 인하여 평균 손실 계수와 스월 수가 증가하지만 형상 손실 계수는 감소한다.

주요어: 공력 손실, 터빈 캐스케이드, 연소기 모사 장치, 연소기 터빈 상호작용, 희석 공기공 유동, 손실 계수

학번: 2019-29557

감사의 글

대학원 생활을 시작하고 시간이 흘러 벌써 졸업을 앞두게 되었습니다. 연구실 생활을 하며, 많은 분들에게 도움을 받으며 지냈습니다. 이 자리를 통해서 감사함을 전해드리려고 합니다.

제가 대학원 과정을 무사히 마치도록 지탱해주신 부모님과 형 감사드립니다. 힘들지는 않는지, 도움을 줄 수 있는 부분이 있는지 물어보신 아버지, 아버지는 제 옆에 계신 그 자체로 힘이 되었고, 용기가 되었습니다. 뒤에서 응원 해주시며, 웃음을 주신 어머니, 어머니의 변함없는 응원 덕에 지금까지 걸어올 수 있었습니다. 마지막으로 언제나 인생의 길잡이 역할을 한 형, 형 덕분에 더 큰 세상을 볼 수 있었습니다. 가족 모두들 감사하고, 사랑합니다.

제가 좋은 연구자가 될 수 있도록 아낌 없이 지도해주신 황원태 지도 교수님께 감사드립니다. 늘 제 의견을 반영해주시고, 저를 믿어주신 덕분에 해낼 수 있었던 과정이었습니다.

함께 고생한 연구실 동료들에게도 감사드립니다. 승찬이형, 훈상이, 구원이형, 재현이형, 규호형, 한준이형, 현균이형, 수현이, 승원이, 무성이, 형우, 상백이, 성광이형, 진무형, 모두에게 감사하고 항상 건강하고 좋은 일이 늘 함께하길 바랍니다.

2021년 1월 27일

지창은